SBAS Corrections for PPP Integrity with Solution Separation

Kazuma Gunning, Juan Blanch, Todd Walter; *Stanford University*

ABSTRACT

An extended Kalman filter (EKF) originally designed for precise point positioning (PPP) has been implemented using GPS broadcast navigation messages and SBAS corrections in conjunction with integrity algorithms originally developed for Advanced Receiver Autonomous Integrity Monitoring (ARAIM) to produce protection levels of less than 10 meters. A new method for handling fault detection and exclusion (FDE) without requiring full reinitialization of the EKF is introduced. This new method maintains low protection levels through FDE.

INTRODUCTION

Precise Point Positioning (PPP) offers high accuracy, global positioning, and there is growing enthusiasm for the application of PPP techniques to safety critical systems [1], [2]. We have shown that PPP, in conjunction with techniques developed for integrity in aviation, can be used to produce meter-level protection levels for static, automotive, and flight scenarios [3]. However, PPP requires real-time, precise orbit and clock corrections, which may not always be available. There have been explorations into using SBAS corrections or broadcast navigation messages for PPP [4], [5], [6], but these have been focused on accuracy rather than integrity. Using SBAS corrections with dual-frequency PPP algorithms, decimeter-level accuracy has been found after convergence. The goal of this paper is to develop and analyze the use of SBAS orbit and clock corrections or simply the broadcast navigation messages with a PPP engine and an integrity algorithm based on solution separation like that used in Advanced RAIM. While SBAS using traditional processing techniques can produce protection levels on the order of tens of meters, it is possible PPP techniques can reduce these protection levels.

The PPP algorithm used is a based on a simple EKF that estimates position, clock, troposphere, float carrier phase ambiguity, and error states. Solution separation requires that multiple filters are run, each of which is tolerant to a fault or set of faults. The number of subsets, i.e. additional filters, is determined by the probability of each fault mode. Solution separation also requires the careful characterization of the error sources so that the nominal covariance produced by the EKF conservatively describes the actual error. One of the goals of this paper will be to analyze the evolution of the orbit and clock error for both SBAS and the broadcast navigation messages so that the covariance matches the true error. In particular, states in the PPP filter estimate the error on that signal, which would take into account the orbit and clock error. Navigation message handover can produce discontinuities in that error, but with the knowledge of when the handover takes place and by staggering the handovers per satellite, the error can be mitigated.

Tests are run for both static and aviation scenarios, using orbit and clock corrections of three varieties: precise orbit and clock products from IGS analysis centers; WAAS SBAS orbit and clock corrections; and broadcast navigation message orbit and clock estimates. Position estimates and protection levels are produced from each case, and these can be compared to non-PPP WAAS solutions and protection levels. Dual frequency measurements are used. For each of these cases, the nominal error characterization and

probability of fault will be assessed. The static data source is a Trimble NetR9 on the roof of the Stanford Aeronautics/Astronautics building in California, USA. The aviation data source is another receiver aboard a Global 5000 aircraft that is owned and operated by the FAA Technical Center in New Jersey, USA.

Estimator design

The PPP algorithm with solution separation is implemented using an extended Kalman filter using dual frequency code and carrier phase measurements. Many of the details of the implementation can be found in [3]. The states estimated are carefully chosen so as to leverage the structure of the problem. The predicted dual frequency code and carrier phase measurements can be modeled as follows:

Dual frequency carrier phase:

$$\Phi_{if}^{(i)} = \left\| x_s^{(i)} - \hat{x}_{rx} \right\| + c\left(\hat{b}_{rx,c} - b_s^{(i)}\right) + m^{(i)}\widehat{\Delta T}^{(i)} + b_{pwu}^{(i)} - \hat{A}^{(i)} + \mathrm{R_m} + \widehat{M}^{(i)} + \hat{\epsilon}_{brdc}^{(i)} + \epsilon^{(i)} \quad (1)$$

Dual frequency code phase:

$$\rho_{if}^{(i)} = \left\| x_s^{(i)} - \hat{x}_{rx} \right\| + c\left(\hat{b}_{rx,c} - b_s^{(i)}\right) + m^{(i)}\widehat{\Delta T}^{(i)} - \widehat{DCB}_{rx}^{(i)} + \mathrm{R_m} + \widehat{M}^{(i)} + \hat{\epsilon}_{brdc}^{(i)} + \epsilon^{(i)} \quad (2)$$

Where

$x_s^{(i)}$- satellite position provided by external precise orbit product

$\hat{x}_{rx}$- estimated receiver position

$\hat{b}_{rx,c}$- estimated receiver clock bias

$b_s^{(i)}$- satellite clock offset provided by external precise orbit product

$m^{(i)}$- tropospheric mapping function

$\widehat{\Delta T}^{(i)}$- estimated delta tropospheric delay

$b_{pwu}^{(i)}$- carrier phase wind-up

$\hat{A}^{(i)}$- estimated float carrier phase ambiguity

$\widehat{M}^{(i)}$- estimated multipath delay on the signal

$\widehat{DCB}_{rx}^{(i)}$- estimated receiver differential code bias per signal (shared across SVs)

$\mathrm{I}^{(i)}$- ionospheric delay/advance

$\mathrm{R_m}$- Other modeled effects. This includes relativistic effects, solid earth tide modeling, satellite antenna phase center offset and variation, ocean loading, modeled tropospheric delay, and any other desired range models. These are strictly modeled and not estimated.

$\hat{\epsilon}_{brdc}^{(i)}$- error due to broadcast navigation message orbit and clock

$\epsilon^{(i)}$- other unaccounted for errors

The estimated states are indicated by a carrot over the symbols. Here, the estimated states include the position, velocity, receiver clock biases, tropospheric delay, carrier phase ambiguities, multipath error, receiver differential code bias, and broadcast orbit and clock error.

This model is mostly typical of a PPP implementation with one significant exception- the state tracking the error contribution of the broadcast orbit and clock on each line of sight. The error contributed by the broadcast orbit and clock can be handled by the filter in one of two ways. The first way is how it is typically handled, where the sigma associated with the navigation message is simply lumped into the measurement sigma. This is generally acceptable for snapshot positioning, but one part of the Kalman filter assumptions is that the measurement error is zero-mean and uncorrelated from epoch to epoch. If we include the broadcast orbit and clock in the not-estimated measurement error term, this assumption will not hold. Figure 1 shows the error in the GPS broadcast navigation message orbit and clock estimates as projected onto a terrestrial user's line of sight. One can see from this figure that the error varies slowly over the course of the day, with jumps only occurring on the changeover from one navigation message to the next. We can leverage this correlation in our estimation of the orbit and clock error by including it as a state for each line of sight and only adding enough process noise to capture the slowly changing error. A characterization of the rate of change of the error in the broadcast orbit and clock is shown later in this paper.

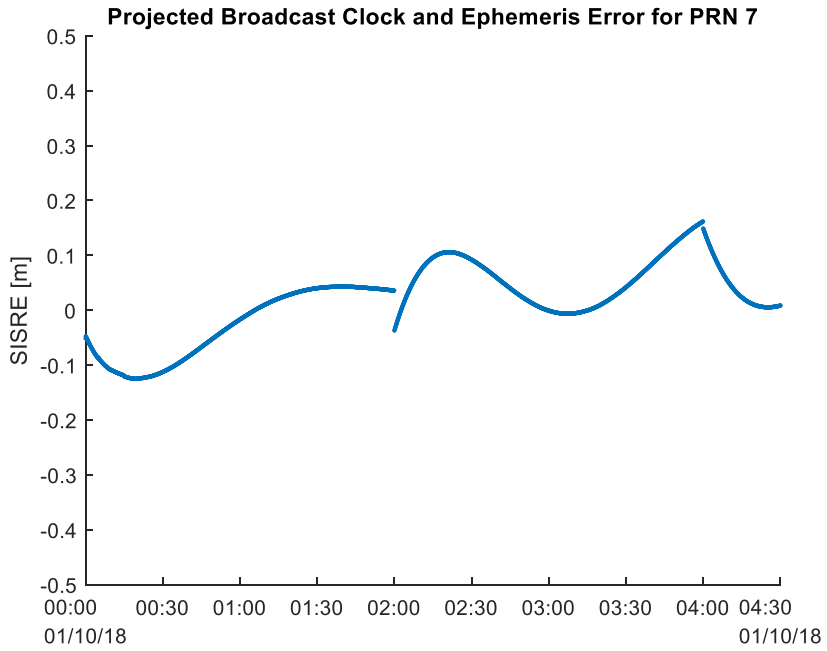

Figure 1: Errors in the GPS broadcast orbit and clock are correlated over time

Integrity algorithm design

We use solution separation-based protection levels derived for Kalman filter navigation solutions as described in [3]. The use of solution separation requires that banks of Kalman filters are run in parallel, each one tolerant to a fault or a set of faults. Much care has been taken to ensure that such banks are not overly computationally demanding, where the main step taken to reduce computational load is the sharing of the computation of modeling across all of the subsets. That is, when the orbit and clock are propagated to the desired time, this is only done once using the all-in-view solution as input, and the orbit and clock state are shared across all subsets. This can be done because in general, these models are not sensitive to the meter or sub-meter level position differences between the subsets. Given the position

estimates and covariances output by the bank of Kalman filters, protection levels are computed using algorithms originally developed for ARAIM which have been since modified for sequential filters.

Ultimately, the protection levels are computed using:

$$PL_{SS,approx2} = \max\left(T_i + Q^{-1}\left(\frac{PHMI}{N * P(H_i)} \right) \sigma^{(i)} \right) \quad (3)$$

Where

Q is the complement of the normal CDF, and Q^{-1} its inverse.

$\sigma^{(i)2}$ is the variance of the estimation error of the subset filter i (the index i=0 corresponds to the all-in-view)

H_i is the fault hypothesis *i*

The threshold T_i is set to meet a predefined probability of false alert P_{fa} under nominal conditions:

$$T_i = Q^{-1}\left(\alpha_i P_{fa} \right) \sigma_{ss}^{(i)} \quad (4)$$

Where

$\sigma_{ss}^{(i)}$ is the standard deviation of the solution separation under nominal conditions.

α_i is the allocation of the probability of false alert to the fault mode. The sum over all modes must not exceed one.

The use of such algorithms requires careful characterization of the environment and the measurements used so that the nominal covariance faithfully reflects the actual error and the fault rates assumed similarly reflect the observed fault rates. The narrow fault rate assumed so far is 10^{-5}, which means that only one-out subsets need be considered.

GPS process noise characterization

The process noise that needs to be added to the clock and ephemeris error states can be estimated through an evaluation of the change in the actual error in the broadcast clock and ephemeris data as projected onto user LOS's. In order to do this, GPS broadcast clock and orbit is compared to precise orbit and clock estimates provided by the National Geospatial-Intelligence Agency (NGA) and the Center for Orbit Determination European (CODE). This process has been described in [7],[8],[9]. The difference between the broadcast and precise estimates is computed at 5 second intervals using GPS clock estimates from CODE, and these differences in the Earth Centered Earth Fixed (ECEF) frame are projected onto the lines of sight of 200 evenly spaced global users over a period from January 1, 2018 to February 28, 2018. The projected error is called the Signal in Space Ranging Error (SISRE). The difference from epoch to epoch of the SISRE at each user location is taken and made into a histogram, taking into account boundaries when there is an IOD handover and binning those samples separately.

The result of this process is shown in Figure 2. The changes in SISRE over time are very different within a navigation message and between consecutive navigation messages. For the core distribution in the blue,

which represents the change in SISRE per second when the navigation message IOD does not change, can be overbounded by a normal distribution with a sigma value of 0.002 m to the 10^{-5} level. If one were to include the IOD crossings, one would need a one-sigma value of 0.16 m, so it is very important to separate the two cases. In fact, because one is able to control when the IOD changeover occurs, we simply reinitialize the estimate of the orbit and clock error when an IOD changeover happens, where the initial uncertainty is the broadcast URA value. This 0.002 m value matches very closely to the GPS SPS guaranteed accuracy for User Range Rate Error (URRE) at the 95% level. The result of this analysis is that the process noise added to the orbit and clock error state is 0.002^2 m^2/s.

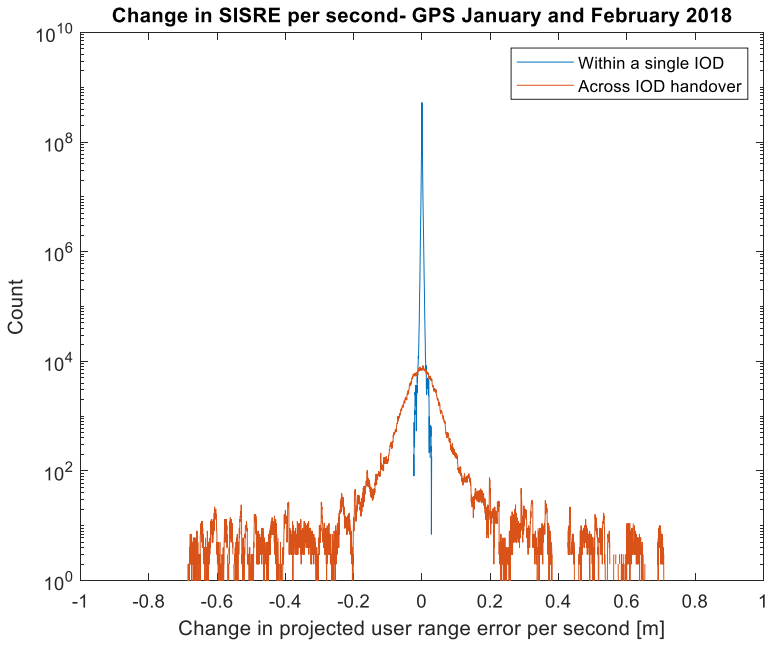

Figure 2: Change in SISRE per second

It is very common for multiple satellites to switch to the next navigation message at the same time at two hour intervals. If we were to reinitialize all of the orbit and clock error estimates at the same time, the filter would essentially go through a soft reset. In order to mitigate this effect, we choose to stagger the changeover from one IOD to the next across the satellites. That is, when new navigation messages are available, only one new navigation message can be used at a time, and the rest of the satellites must use their older, but still valid, navigation messages. After a certain amount of time, which is set to 10 seconds, another PRN can next switch to a new navigation message. This reduces the impact of the added process noise needed to change from one navigation message to the next. Figure 3 depicts this process, where each dashed line indicates the IODE of a different GPS satellite. One satellite performs an IODE handover at the 10 second mark, another at 20 seconds, and so on.

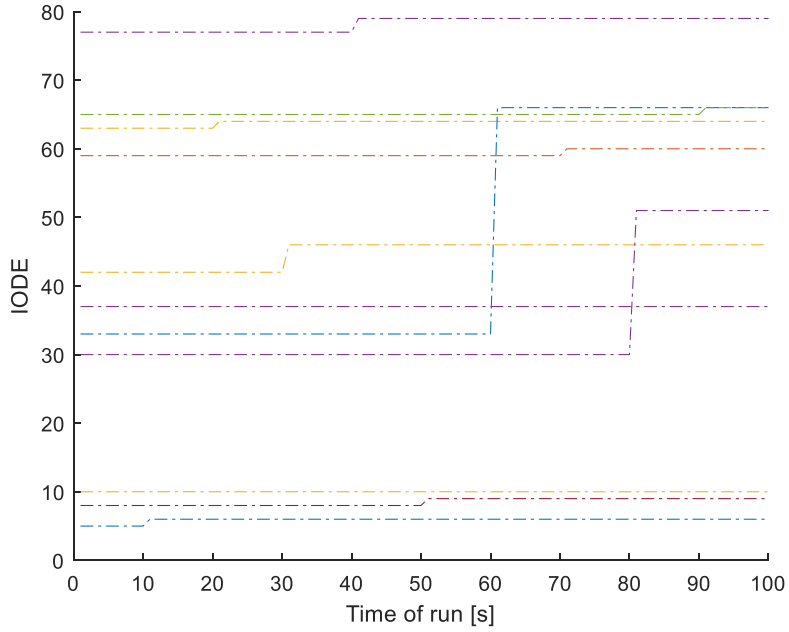

Figure 3: Staggered IODE Changeover

Inclusion of WAAS Corrections

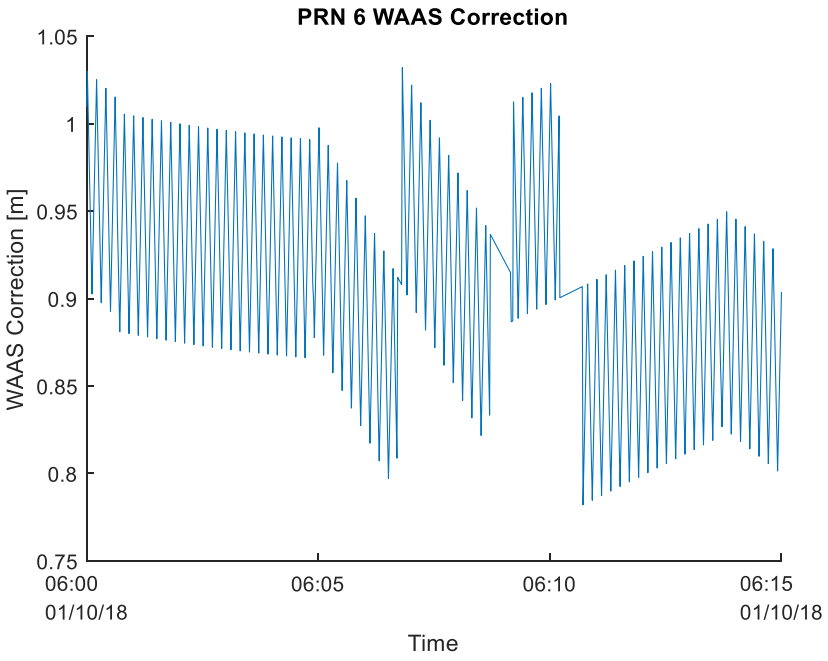

Figure 4: WAAS Broadcast Orbit and Clock Corrections

WAAS corrections are not directly applied to either the pseudorange measurements for reasons that can be seen in Figure 4, which shows the line of sight orbit and clock corrections for an arbitrary user and PRN over a fifteen-minute period. The range-rate corrections in particular make it such that, if the corrections

were directly applied to the pseudorange and code measurements, a large amount of process noise would need to be added into the broadcast error state at each epoch, which would lead to increased uncertainty in the overall covariance. Even without the range-rate corrections, the quantization of the corrections would lead to a similar effect, and because the corrections come at such a high rate, staggering the correction changeover as is done for the broadcast ephemeris becomes problematic. So, instead, the corrections are inserted into the filter as direct measurements of the line of sight broadcast ephemeris error. Equations 5 shows the simple measurement model, where δr_{WAAS} is used as a direct measurement of the broadcast error. Equation 6 shows that the measurement noise used is provided by σ_{FLT},which is here the σ_{UDRE} inflated by the covariance projection onto the specific line of sight, where the covariance is provided in WAAS Message Type 28. This measurement model is likely slightly optimistic, as it assumes that the measurement error on the corrections conforms to the Kalman filter assumptions that they are zero-mean and uncorrelated over time. As the WAAS orbit and clock estimator is a "faster" system than that of the GPS control segment because it does not have global reference stations and thus must quickly make adjustments to the estimates based on real time measurements, these assumptions may not be very far off. However, this will need to be further investigated in future works.

$$\text{Measurement model:} \quad \hat{\epsilon}_{brdc}^{(i)} = \delta r_{WAAS} \tag{5}$$

$$\text{Measurement noise:} \quad \sigma_{\delta r_{WAAS}}^{(i)} = \sigma_{FLT} \tag{6}$$

The WAAS corrections used in this paper were provided by the FTP site of the National Satellite Test Bed (NSTB) [10], which contains years of daily logs of the WAAS messages broadcast by the various geostationary satellites. These logs are downloaded and are at this stage binary data, which can then be parsed and propagated using MATLAB tools adapted [11] and built for handling WAAS corrections.

RESULTS

Three sets of results are provided: a nominal static scenario, a flight scenario, and a static scenario with an injected fault on a single PRN. Each of the scenarios uses dual frequency code and carrier with only GPS.

Static scenario

The first set of results comes from a Trimble NetR9 on the roof of the Aeronautics/Astronautics building at Stanford University. It is 3 hours of 1 Hz data on GPS L1 C/A and semi-codeless L2P. As this receiver is a member of the International GNSS Service's (IGS) Multi-GNSS Experiment (MGEX) network, a daily high accuracy solution is produced. The daily MGEX solution is used as the truth reference in this section.

Figure 5 shows the position error and protection levels found using only the GPS broadcast navigation message, using WAAS corrections in addition to the broadcast navigation message, and using full PPP implementation. As is typical of PPP techniques that rely on estimating float carrier phase ambiguities, there is a convergence period in the protection levels for all three cases. First discussing the case using the broadcast navigation message without WAAS corrections, the convergence is very slow. The protection levels do not seem to reach any sort of steady state until after two hours have passed, due to the additional process noise and overall uncertainty provided by the navigation message error augmented states. However, within 15 minutes, the protection levels in the East and North directions are under 10 meters, and the vertical protection level is under 15 meters. After two hours of convergence, the

protection levels in the East, North, and up directions are approximately 6 meters, 3.5 meters, and 7 meters, respectively.

The protection levels produced using WAAS corrections with the broadcast navigation message are close to those produced using the full PPP implementation with external corrections. Convergence occurs in the first 30 minutes, and the WAAS protection levels are generally within one meter of the PPP protection levels, at approximately 3 meters in the East and North directions, and 4 meters in the up direction. As previously mentioned, these protection levels use an optimistic measurement model. However, the accuracy is drastically increased using WAAS corrections to better than 15 centimeters RMS horizontal, and the position error normalized by the nominal covariance output by the all-in-view (AIV) filter remains very conservative. Finally, the error also does not exceed a small fraction of the protection level at any point during the run.

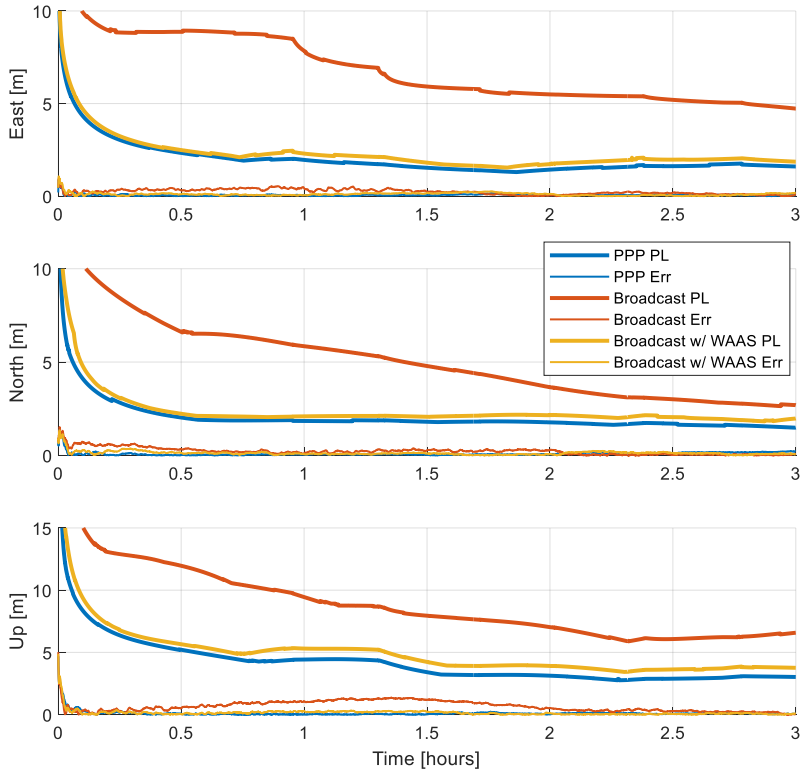

Figure 5: Position error and protection levels using broadcast navigation data

Flight results

This section describes results from flight data collected on an FAA Global 5000 aircraft. The data shown in Figure 6 consists of flight data from a roughly two-hour flight near Philadelphia, Pennsylvania on June 30, 2017. The receiver used was a Trimble BD935, and the signals used were GPS L1 C/A and L2P semi-codeless. The truth against which the position estimates were compared were provided by the Natural Resources Canada Reference System Precise Point Positioning (CSRS-PPP) service.

Figure 6 shows the position error and protection levels derived for this scenario using only the GPS broadcast orbit and clock from the navigation message. As with the static data, there is a convergence

period, where this period is longest for the broadcast navigation message data and under 30 minutes for the WAAS correction and PPP cases. The WAAS correction protection levels again rival those of the full PPP case. The broadcast-only protection levels are consistently less than 15 meters in every direction, which is a significant improvement over traditional RAIM or even SBAS protection levels, which are typically in the tens of meter range.

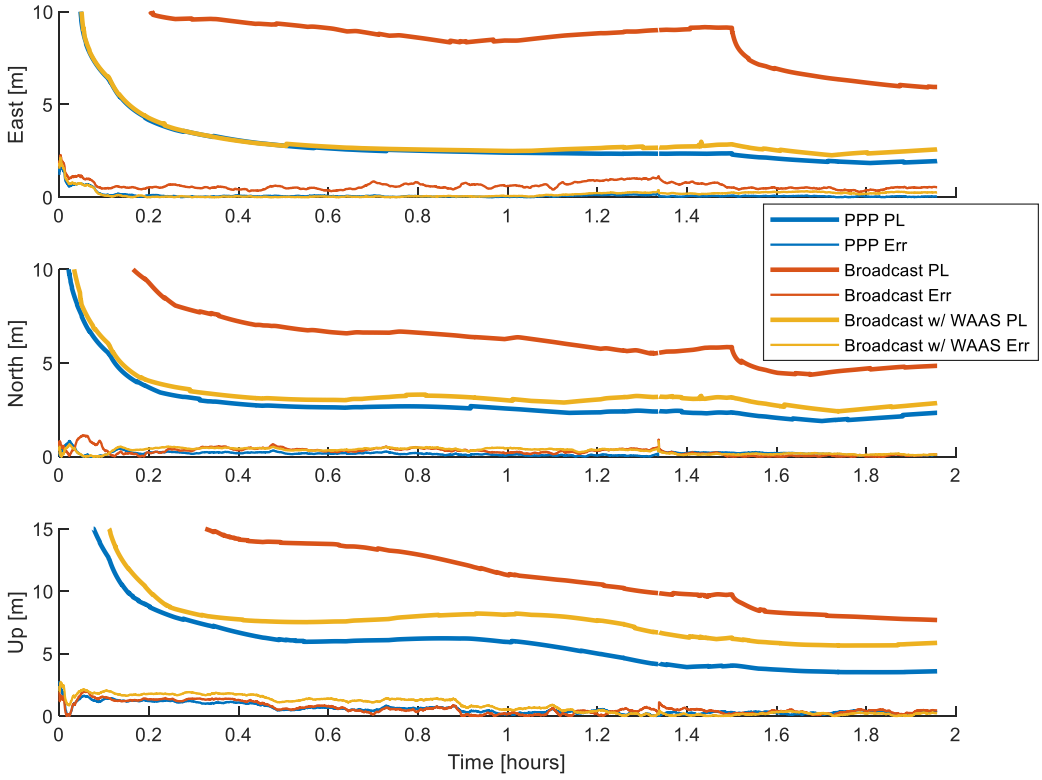

Figure 6: Position error and protection levels for flight data

FAULT DETECTION AND EXCLUSION (FDE)

A fault is injected into the static scenario in order to check that the fault detection and exclusion abilities of the system operate correctly. Two different methods are employed to compute the subsets and associated protection levels after fault exclusion. The injected fault is modeled after an observed GPS fault from 2010.

The fault occurred on PRN 30 on February 22, 2010 and is shown in Figure 7 and Figure 8. Figure 7 shows the broadcast clock and ephemeris error split into the radial, along-track, cross-track, and clock components as well as the maximum projected error (MPE), which is the worst-case error experienced by a terrestrial user. A fault begins at approximately 21:00 (indicated by the red shaded area), and the fault is caused by a clock runoff. This can be seen in Figure 8, where the broadcast clock bias (red circles) and the true clock bias (blue dots) start to diverge as the onboard clock experiences a frequency offset leading to a ramp error. This fault can be modeled as a ramp of approximately 50 meters/hour. The fault is injected into he static scenario data by adding such a ramp to all measurements from a single PRN starting 20 minutes into the run.

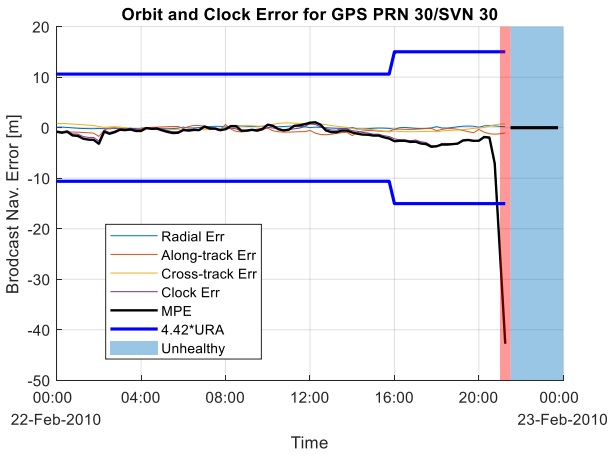

Figure 7: Observed GPS fault from 2010

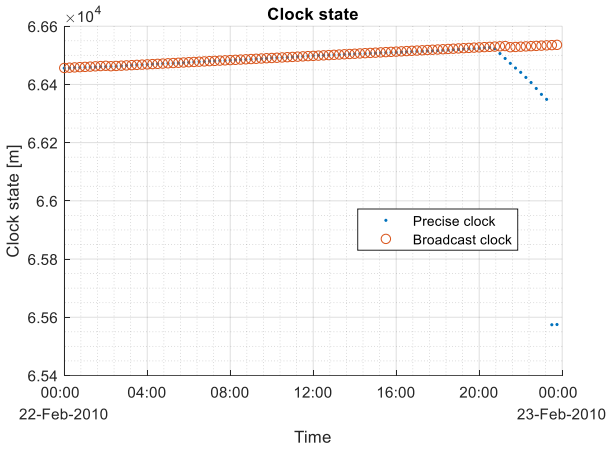

Figure 8: Precise and broadcast clock bias from PRN 30 fault

The following section describes two methods for reinitializing the PPP filters once a fault has been detected and excluded. The original method, as used in [3], requires that the entire filter, including the subset filters, be completely restarted, leading to a sizable jump in the protection levels. The new method to be described relies on carrying extra subset filters that are not used in the protection level computations and are only used in the FDE process. The two methods will be described here.

Original method for FDE

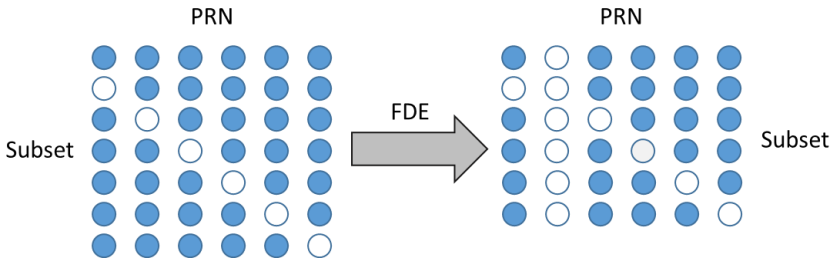

Figure 9: Measurement usage diagram for original fault detection and exclusion method

The first method involves a simple reinitialization of the AIV and subset filters after fault detection and exclusion. The only subsets that are computed are those required to produce protection levels at the current epoch. The left part of Figure 9 shows a diagram of measurement usage for the all in view (top row) and the other subsets (rows 2 onward). In the diagram, each row is a different subset, and each column is a different PRN, where the filled blue circles indicate that the measurement is used, and the empty circles indicate that the measurement is excluded. For solution separation considering only one-out subsets, all that is needed to produce a protection level is the subsets included in the left diagram.

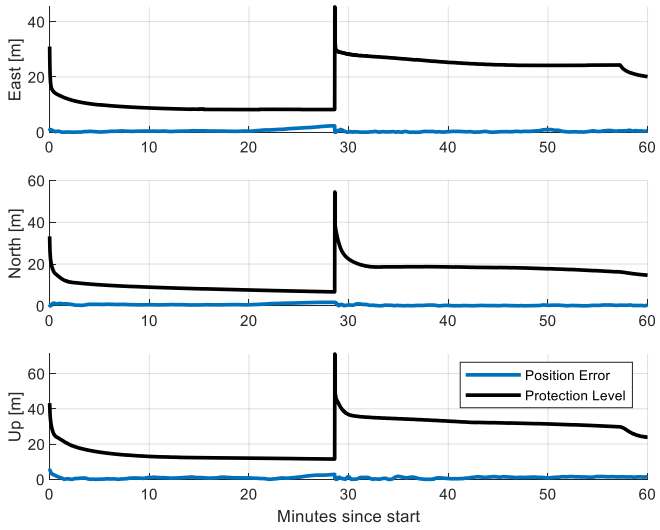

Figure 10: Position error and protection levels given injected ramp fault and original FDE method

Figure 10 shows the results of using this method given an injected fault as described previously. Twenty minutes into the run, the ramp fault begins, which can be seen in the growth in the position error. Just before the thirty-minute mark, the growth in the solution separations exceeds the computed threshold, indicating that a fault has been detected. The fault, on PRN 2, is identified, and the new desired AIV and subsets must have PRN 2 excluded. This is shown on the right side of Figure 9. The new AIV is actually a subset of the original set, but because none of the new subsets have been tracked previously, the already tracked AIV cannot be used, and the entire filter must be reinitialized. The reason that the previously tracked AIV cannot be used is that if new subsets were spawned given an already converged AIV, those subsets would not be tolerant to faults on measurements that have already been included in the AIV solution. Once the filters are reinitialized, the protection level spikes, and because of the weakened geometry due the missing PRN, the protection levels take longer than usual to converge again.

New method for FDE with "on-deck" filters

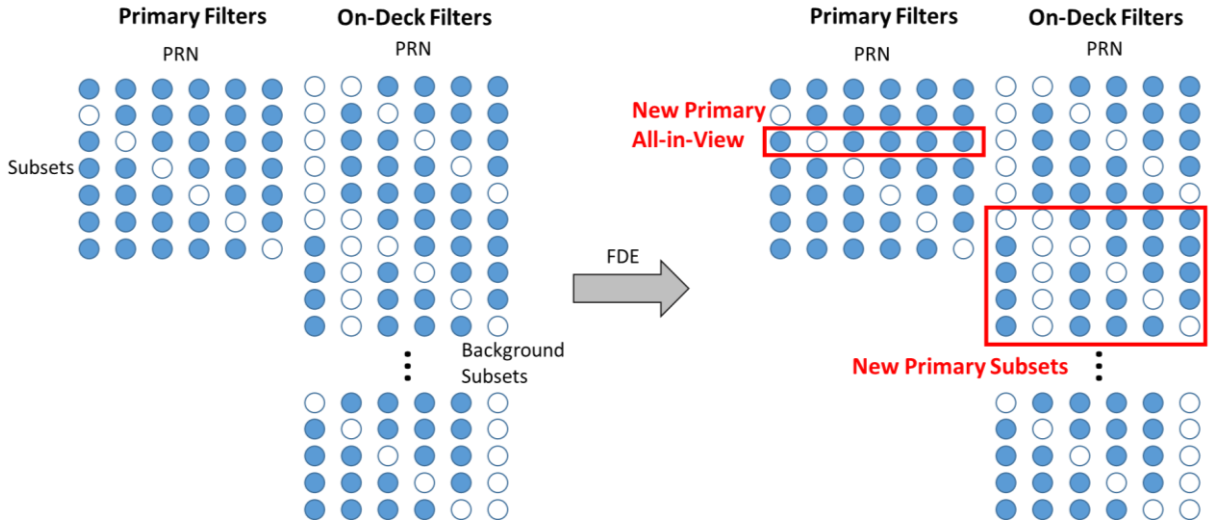

Figure 11: Measurement usage diagram for original fault detection and exclusion method

In order to avoid the large jump in protection levels upon reinitializing the filters after FDE, a new process has been developed wherein "on-deck" subsets are produced and are only used in case of FDE. Essentially, if we are only concerned with one-out subsets as we have been, then the on-deck subsets would be the two-out subsets, as shown in the left side of Figure 11. These subsets are not included in the protection level computations.

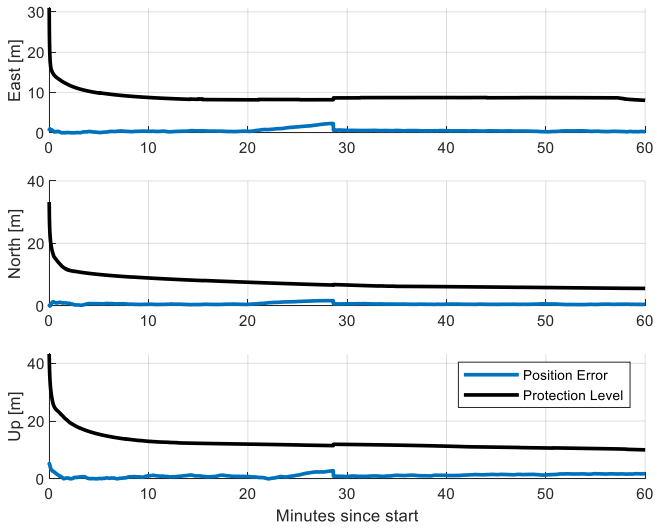

Figure 12: Position error and protection levels given injected ramp fault and new FDE method

Figure 12 shows the results given the injected fault and the new FDE method involving the on-deck subsets. At the same point as in Figure 10, a fault is detected. However, the filters do not need to be reinitialized because the new AIV and subsets have been tracked all along. These filters are highlighted by the red boxes on the right of Figure 11. The new on-deck filters need to be reinitialized at this point, but as long as another fault is not detected before those filters converge, this does not impact the protection levels. The new AIV was one of the original subsets filters, and the new primary subsets were already converged in the on-deck filters. It is, of course, computationally expensive to carry around the on-deck filters, but techniques such as grouping of the subsets have been explored [12], [13], which can dramatically reduce the computational load. After FDE, the protection levels are slightly increased due to the weakened geometry, but most importantly, they are already converged.

CONCLUSION

A system has been developed to produce horizontal protection levels of less than 10 meters after convergence using only GPS broadcast navigation messages and external inputs. The navigation algorithm relies on an extended Kalman filter and with states that track the error contribution of the broadcast orbit and clock. The integrity algorithm uses solution separation with protection levels similar to those used for ARAIM. With WAAS corrections, protection levels rivaling those of a full PPP system have been found, and broadcast-only protection levels have been found that are far lower than those produced by SBAS or traditional RAIM. Finally, a new method for maintaining converged protection levels through FDE for EKF-based solution separation has been introduced. These methods provide an opportunity for much lower protection levels than have been previously shown given only data broadcast on open satellite signals.

REFERENCES

[1] Madrid, P. F. Navarro, Fernández, L. Martínez, López, M. Alonso, Samper, M.D. Laínez, Merino, M.M. Romay, "PPP Integrity for Advanced Applications, Including Field Trials with Galileo, Geodetic and Low-Cost Receivers, and a Preliminary Safety Analysis," *Proceedings of the 29th International Technical Meeting of The Satellite Division of the Institute of Navigation (ION GNSS+ 2016)*, Portland, Oregon, September 2016, pp. 3332-3354.

[2] D. Calle, E. Carbonell, P. Navarro, P. Roldán, I. Rodríguez, G. Tobías, "Facing the Challenges of PPP: Convergence Time, Integrity and Improved Robustness" *Proceedings of the 31th International Technical Meeting of The Satellite Division of the Institute of Navigation (ION GNSS+ 2018)*,Miami, Florida, September 2018.

[3] K. Gunning, J. Blanch, T. Walter, L. de Groot, L. Norman, "Hexagon Positioning Intelligence, Canada Design and Evaluation of Integrity Algorithms for PPP in Kinematic Applications" *Proceedings of the 31th International Technical Meeting of The Satellite Division of the Institute of Navigation (ION GNSS+ 2018)*,Miami, Florida, September 2018.

[4] Rho, Hyunho, and Richard B. Langley. "The usefulness of WADGPS satellite orbit and clock corrections for dual-frequency precise point positioning." *Proc ION GNSS*. Vol. 2007. 2007.

[5] Heßelbarth, Anja, and Lambert Wanninger. "SBAS orbit and satellite clock corrections for precise point positioning." *GPS solutions* 17.4 (2013): 465-473.

[6] Zhao, Yu, et al. "A novel SBAS-assisted single-frequency precise point positioning method." *China Satellite Navigation Conference (CSNC) 2016 Proceedings: Volume III*. Springer, Singapore, 2016.

[7] T. Walter and J. Blanch, "Characterization of GPS Clock and Ephemeris Errors to Support ARAIM," in Proceedings of the ION 2015 Pacific PNT Meeting, Honolulu, Hawaii, 2015, pp. 920-931.

[8] S. Perea Diaz, M. Meurer, M. Rippl, B. Belabbas, M. Joerger, and B. Pervan, "URA/SISA Analysis for GPS-Galileo ARAIM Integrity Support Message," 2015.

[9] O. Montenbruck, P. Steigenberger, and A. Hauschild, "Broadcast versus precise ephemerides: a multi-GNSS perspective," GPS Solutions, vol. 19, no. 2, pp. 321-333, 2015// 2015.

[10] "NSTB Data Download." *William J. Hughes Technical Center WAAS Test Team*, Federal Aviation Administration, ftp://ftp.nstb.tc.faa.gov/pub/NSTB_data/.

[11] Do, Juyong. "Stanford GPS/GNSS Matlab Platform." *Stanford GPS Lab*, Stanford University, gps.stanford.edu/sgmp.

[12] Blanch, Juan, et al. "Reducing Computational Load in Solution Separation for Kalman Filters and an Application to PPP Integrity." *Intitute of Navigation International Technical Meeting*, 31 Jan. 2019.

[13] Blanch, Juan, Walter, Todd, Enge, Per, "Fixed Subset Selection to Reduce Advanced RAIM Complexity," *Proceedings of the 2018 International Technical Meeting of The Institute of Navigation*, Reston, Virginia, January 2018, pp. 88-98.